RAFT Polymerization of MMA in the Channels of Different Mesoporous Materials

Tao Xue
Guilin University of Technology
Yan Wei
Guilin University of Technology
Caili Yu
Guilin University of Technology
Faai Zhang (Zhangfaai@glut.edu.cn)
Guilin University of Technology

Research Article

Keywords: mesoporous materials, RAFT polymerization, Confined space, Microreactor

Posted Date: April 21st, 2022

DOI: https://doi.org/10.21203/rs.3.rs-1559941/v1

Abstract

A serial of mesoporous materials (MS), i.e., rod-liked and spherical SBA-15, spherical MCM-41 and MCM-48 were successfully synthesized and modified by silane coupling agent KH550 then utilized as a microreactor for reversible addition–fragmentation chain transfer (RAFT) polymerization of methyl methacrylate (MMA) using a xanthate as a chain transfer agent and AIBN as an initiator. The structures, morphologies and properties of the obtained polymers and composites were characterized by Fourier transform infrared spectroscopy, scanning electron microscopy, nitrogen adsorption and desorption, thermogravimetry analysis, gel permeation chromatograph, and hydrogen nuclear magnetic resonance. Results showed that compared with conventional MS, modified MS featured with lower specific surface area and pore volume while maintained the original morphological structure. Owing to confinement effects, PMMAs obtained from internal mesoporous channels featured with higher molecule weight and initial thermal decomposition temperature than these from conventional RAFT polymerization, especially, the PMMA obtained from the spherical SBA-15 and modified MCM-48 exhibited the highest molecule weight.

Introduction

Mesoporous materials (MS), notably those made of silica or silicon, are attracting great interest in the field of microreactor [1–3]. Thanks to their excellent porous structure and characteristics such as tractable surface morphology, consistent and flexible pore size, spacious interior space that can protect interaction independence from external environment and their compatibility, MS features prominently in nanodevices [4, 5], drug delivery [6–8], adsorption [9, 10], separation [11, 12], photonic waveguides [13] and biometrics [14].

It's generally accepted that living free radical polymerization is better than the traditional one under the constant conditions because the latter one limits the ending polymer’s molecular weight, polydispersity, and constructive multiplicity. However, the traditional living free radical polymerization suffers from a series of weakness, including an expensive and noxious irreplaceable reagent, a few viable monomers, harsh polymerization conditions and quite troublesome post-processing of product [15, 16].

In order to enhance the efficiency and decrease cost, a new type of the living free-radical polymerization was emerged: reversible addition fragmentation transfer (RAFT) polymerization which exhibited a reversible transfer process between the active and dormant chains controlled by a chain transfer agent with a functional group that can yield a powerful control of the polymerization. After immense exploration in reaction by the academic circle, RAFT polymerization seems to be the most versatile one with regard to monomer selection, polymeric configuration and reaction condition among a great number of the living free radical polymerization.

MS provides an independent and restrictive space, which can lead free radical to grow smoothly and better control of the termination of reaction [17, 18]. An enormous deal of modifiable MS was reported in

literature for diverse living radical polymerization to obtain more superb and relevant products. Xu [19] selected mesoporous SBA-15 with various pore sizes as microreactors to lead methyl methacrylate (MMA) reaction by RAFT polymerization for the sake of seeking a novel and pragmatic approach to create polymer microstructure for a series of application, such as in drug release. Chen [20] utilized mesoporous silica SBA-15 as carrier to graft polymerization of functional monomer glycidyl methacrylate (GMA) under the mixed solvents via activators regenerated by electron transfer atom transfer radical polymerization (ARGET ATRP) method and found that the PGMA brushes grafted SBA-15 were able to serve as a talented reactive platform for deeper surface modification or functionalization. In the report of Joshi [21], an extraordinary integration was given to both the mesoporous silica nanoparticles and the RAFT agent, an alternative stepwise approach for co-condensation in the presence of hexadecyl trimethyl ammonium bromide was exploited, and further used the mesoporous silica nanoparticles containing RAFT agent for surface-initiated RAFT polymerization of several monomers.

Owing to the shape-selective and confinement effect, there is generally accepted that morphology of the mesoporous is one of the most significant influencing factors for the macroscopic application, as each MS owns its unique advantages, in particular spherical MS invariably has surpass stability and ruggedness while rod-liked MS possess the order character. Du [10] designed a facile method to control and fabricate mesoporous carbon materials (MC) with different morphologies and proved that MC with regular spherical morphology showed noteworthy adsorption capacity engendered attractive prospects in treating waste water. Dan [22] prepared a class of SBA-15 which were employed to adsorb uranium from aqueous solution and identified that the platelet-like morphology SBA-15 exhibited absolutely rapid and high capacity adsorption of uranium. Furthermore, as a microreactor, the type of both the monomer wrapped internal and the MS which supplied an immune location for the former is fairly important condition for mesoporous when polymerization happened. Zeng [23] chose three monomers (MMA, GMA and styrene) with different polarities to react in the interior of SBA-15 in order to probe the confinement dimensions on the resulting polymer properties.Moritz[24] synthesized three typical mesoporous (SBA-15, PHTS and MCM-41) functionalized with a sulfonic acid derivative and were applied successfully as the carriers for the poorly water-soluble drug.

We are interested in the RAFT polymerization in a confined space such as various MS. In order to comprehend the effect of MS on the polymerization, the solution RAFT polymerization of MMA in different MS (rod-liked and spherical SBA-15, spherical MCM-41 and MCM-48, and silane coupling agent KH550 functionalized SBA-15) were carried out. The polymers obtained from the internal channels of the MS were characterized.

Experimental

Materials

Pluronic P123 (EO20 PO70 EO20, Mn = 5800) and mesitylene (TMB, AR) were purchased from Sigma–Aldrich Co. (USA). MMA (CP), potassium chloride (KCl, AR), methanol (AR), toluene (AR), sodium

hydroxide (NaOH, AR), ammonia water ($NH3{\cdot}H_2O$, 25–28%), tetraethyl orthosilicate (TEOS, AR), hydrofluoric acid (HF, ≥ 40%) hydrochloric acid (HCl, 36–38%), and tetrahydrofuran (THF, AR) were all purchased from Xilong Science and Technology Co. in Shantou, Guangdong Province (China). MMA was treated with 10% aqueous NaOH solution for three times to remove the inhibitor, then washed with distilled water to be neutral, dried with anhydrous $CaCl_2$, and distilled under reduced pressure. Anhydrous ethanol (AR) was purchased from Guangdong Guanghua Technology Co., Ltd. (Shantou, Guangdong province, China). Azodiisobutyronitrile (AIBN, AR), purchased from Tianjin Guangfu Fine Chemical Research Institute (Tianjing, China), was used after recrystallization from absolute ethanol. Potassium ethyl xanthate (AR) and ethyl 2-bromopropionate (AR) were purchased from Aladdin Industrial Corporation (Shanghai, China) and used directly. γ-aminopropyltriethoxysilane (KH550, CP) was purchased from Nanjing Xiangfei Chemical Research Institute (Nanjing, Jiangsu province, China). Ethyl xanthate ethyl propionate was synthesized according to the reported work. All other chemicals were used as received without further purification.

Preparation of rod-liked SBA-15

Typically [25], 2.5 g of P123 was dissolved in 2 mol/L HCl at 35.5°C, stirred at 300 r/min for at least 6 h. When the dissolution was complete, 5.5 g of TEOS, a silica source, was added (dropwise within 10 min) and stirred for 24 h. Subsequently, it was put into a hydrothermal reactor and crystallized at 100°C for 24 h. The product was extracted, washed, and dried in a constant temperature drying oven at 40°C. Finally, the white powder was put into a muffle furnace and calcined at 2°C/min to 550°C for 6 h. The template agent was removed by roasting to obtain the rod-liked MS R-SBA-15.

Preparation of spherical SBA-15

In a typical synthesis [26], 4.2 g of P123 and 3.0 g of KCl was dissolved in 2 mol/L HCl at 35.5°C, then stirred the solution at 300 r/min for at least 6 h. After the P123 was fully dissolved (the solution was completely clarified), cooled to 28°C and added 3.0 g of TMB, continuous stirring for 12 h, then slowly added 8.6 g of TEOS drop by drop. The white powder was finally calcined in a muffle furnace and heated to 550°C at 2°C/min for 6 h. The spherical MS S-SBA-15 was obtained by roasting to remove the template agent.

Preparation of spherical MCM-41

In a typical synthesis [27], adding 3.75 g CTAB to 71 ml of water and stirred at room temperature until completely dissolved, then 25.8 g of ammonia water and 90 g of ethanol was added and stirred at 500 rpm for 30 min, after that, 7.5 g of TEOS was added dropwise within 10 min, and heated the mixture to 25°C with stirring at 500 rpm for 3 h, the product was dried in a thermostat at 60°C for 24 h. Finally, the white product was calcined in a muffle furnace at 2°C/min for 5 h at 550°C to obtain spherical MCM-41.

Preparation of spherical MCM-48

In a typical synthesis [28], 2.4 g (6.59 mmol) of CTAB was dissolved in 50 g of deionized water, then 50 mL of ethanol and 12 mL of ammonia was added and stirred at room temperature for 5 h (300 r/min),

then 3.4 g (16.3 mmol) of TEOS (dropwise in 10 min) was added and stirred at 450 r/min for 2 h, after that the mixture was crystallized for 24 h, filtered. The spherical MCM-48 was obtained by slowly increasing the temperature (2°C/min) to 600°C for 6 h and removing the template agent.

Functionalization of MS

The different MS R-SBA-15, S-SBA-15, MCM-41 and MCM-48 were modified with silane coupling agent KH550 in a typical synthesis [29], 1.0 g of MS activated by 2 mol/L dilute hydrochloric acid was weighed into a 50 mL single mouth flask, 15 mL of toluene was added then ultrasonic treated at room temperature for 30 min to achieve uniform dispersion. After the reaction, the MS was naturally cooled to room temperature, filtered, washed 4–5 times with toluene (to remove the silane coupling agent from the outer surface of the MS) and dried at 60°C for 24 h to obtain modified MS (denoted as M-MS).

RAFT polymerization of MMA in different MS

Different MS were selected as microreactors and the RAFT solution polymerization of MMA was carried out inside the pore channels. Mesoporous silica (0.5 g) was added into an 50 ml round bottom flask, degassed under vacuum at 150°C for 5 h, then maintained vacuum and cooled down to room temperature, followed by adding the configured mixed solution (toluene 7 ml, MMA 5.2 ml, AIBN 0.0164 g, CTA 0.111 g), and stirred under vacuum for 3 h to fully immerse the mixture into the pore channel of the mesoporous silica under nitrogen atmosphere. The reaction was carried out in an oil bath at 80°C for 12 h. After the reaction was completed, it was cooled down to room temperature, THF was added and stirred for 24 h to fully dissolve the polymer on the surface of the MS, then the mixture was filtered and washed 3 times with THF, and the crude product was dried at 60°C. The crude product was then extracted with THF for 12 h to remove the polymer attached to the outer surface of the MS, and dried to obtain MS/PMMA composites (i.e.R-SBA-15/PMMA, S-SBA-15/PMMA, MCM-41/PMMA, MCM-48/ PMMA). The composites prepared from silane coupling agent KH550 modified MS were recorded as M-MS/PMMA (i.e.M-R-SBA-15/PMMA, M-S-SBA-15/PMMA, M-MCM-41/PMMA, M-MCM-48/PMMA).

PMMA obtained inside the mesoporous channels

The composites MS/PMMA and M-MS/PMMA were etched firstly with aqueous HF solution at a mass concentration of 5%, followed by centrifugal separation, washing with deionized water and drying, the PMMAs inside the pores of the MS were obtained, which were noted as PMMA in R-SBA-15, PMMA in S-SBA-15, PMMA in MCM-41, PMMA in MCM-48, PMMA in M-R-SBA-15, PMMA in M-S-SBA-15, PMMA in M-MCM-41, PMMA in M-MCM-48, respectively.

Characterization

A field emission scanning electron microscopy (SEM, JSM-6380LV from Japan Electronics Co., Ltd) was used to observe the morphology of the mesoporous silica and MS/PMMA composites at 5–10 KV after spraying the specimens with gold. Nitrogen adsorption–desorption isotherms curves were obtained using a Micrometrics TriStar II 3020. Samples were degassed under vacuum at 200°C (for silica) or 120°C (for synthetic composites) before adsorption measurements. The specific surface area was determined using

the BET method. The total pore volume was calculated from the amount adsorbed at a relative pressure of 0.99. The pore size distribution was calculated using the BJH method for cylindrical mesopores. The thermal decomposition behaviors of the MS, MS/PMMA, M-MS/PMMA composites, and PMMA obtained from MS were examined by means of thermogravimetric analysis (TGA) with a heating rate of 10 K/ min in nitrogen atmosphere on a TA Q500 (USA). The structures of the samples were characterized on a Nicolet-205 Fourier transform infrared spectrometer (FTIR) from 400 to 4000 cm^{-1} by the KBr tablet methods and Proton magnetic resonance ($^{1}H/^{13}C$ NMR) spectroscopy were taken on an Avance 500 MHz spectrometer (Bruker, Switzerland) using $CDCl_3$ as solvent and tetramethylsilane (TMS) as internal standard. The molecular weight and MWD of the polymers were measured on a Malvern Model 270 gel permeation chromatograph (GPC) equipped with T6000 microstyragel columns, refractive detector, light scattering detector and viscosity detector and THF was used as an eluent at a flow rate of 1.0 $mL \cdot min^{-1}$.

Results And Discussion

Morphology

Fig. 1 shows SEM images of the different MS and MS/PMMA composites. As can be seen from Fig. 1, different morphologies and types of MS are successfully prepared, namely, rod-liked R-SBA-15, spherical S-SBA-15, spherical MCM-41 and MCM-48. The length of rod-liked SBA-15 is above 1 μm and the width is around 0.3-0.5 μm, the particle size of spherical SBA-15 is about 3 μm. Whereas the particle sizes of the spherical MCM-41 and MCM-48 are in the range of 0.2 to 0.7 μm and 0.2 to 0.5 μm, respectively. The SEM images of the MS/PMMA composites show that the surface are clean and smooth with no obvious attachments, indicating that the complete removal of outside polymer from the washing step. In addition, in the images of R-SBA-15/PMMA (A2), S-SBA-15/PMMA (B2), MCM-41/PMMA (C2) and MCM-48/PMMA (D2), it is obvious that morphologies of the MS/PMMAs obtained after polymerization in the channels of the MS replicate the framework of MS, which are consistent with previous reports [30,31].

Nitrogen adsorption–desorption isotherms

The nitrogen adsorption–desorption isotherms of the different MS, M-MS, MS/PMMA and M-MS/PMMA composites are depicted in Fig. 2. Tab. 1 lists the parameters of them. In combination with Fig. 2 and Tab. 1, comparing the pore parameters and adsorption isotherm curves of the MS and M-MS, we can pinpoint that the silane coupling agent modified MS (M-MS) have the same type of isotherm adsorption curves, lower liquid nitrogen adsorption, and reduced specific surface areas and pore volumes, indicating that the silane coupling agent was successfully grafted within the mesoporous pore channel.

As can be seen from Fig. 2(a), the hysteresis loop of R-SBA-15/PMMA is smaller than that of R-SBA-15 and the adsorption desorption temperature line also belongs to type IV with an H1 hysteresis loop, whereas the adsorption desorption isotherm curves of M-R-SBA-15 and M-R-SBA-15/PMMA belong to type II with a decrease in both specific surface area and pore volume, which indicates that MMA was successfully adsorbed into the mesoporous pore channel and polymerization took place [32]. In addition,

from the nitrogen adsorption/desorption curves in Fig. 2(c), the isotherms of S-SBA-15 and M-S-SBA-15 both belong to type IV with H1 lagging loop, and at the same time the isotherms of S-SBA-15/PMMA and M-S-SBA-15/PMMA also belong to type IV with H1 lagging loop, however the adsorption volumes decrease and the lagging loop becomes smaller, demonstrating that the mesoporous structure of S-SBA-15 and M-S-SBA-15 are still retained and some of the pores are filled with PMMA. Both the S-SBA-15/PMMA and M-S-SBA-15/PMMA composites show a decrease in specific surface areas and pore volumes, while the average porosity calculated based on the BJH model shows a slight increase, which could be attributed to the generated polymer filling the micropores in S-SBA-15 [33].

The isothermal adsorption curves for MCM-48 and MCM-41 are of type IV with a H4 lagging loop, which are caused by the small pore sizes of these two MSs and the presence of slight defects in the mesopore channels [34]. Due to the fact that the surfaces of the mesopore channels have been modified by organic functional groups, the specific surface areas and pore volumes of the M-MCM-41 and M-MCM-48 reduce greatly; in addition, both the specific surface areas and pore volumes of the MS/PMMA and M-MS/PMMA composites decrease further, because the PMMAs are generated in the channels of the MS and M-MS. Furthermore, the adsorption/desorption isotherms of the modified M-MCM-41, M-MCM-48 and the MS/PMMA composites belong to type I [35,36].

Tab. 1 Pore structural parameters of MS, MS/PMMA composites and M-MS/PMMA composite

Samples	Specific surface area/ BET (m^2/g)	Total volume (m^3/g)	Average pore width/ BJH (nm)
R-SBA-15	806.9	1.07	5.72
R-SBA-15/PMMA	79.1	0.20	8.18
M-R-SBA-15	24.4	0.06	6.62
M-R-SBA-15/PMMA	24.0	0.07	7.44
S-SBA-15	365.2	1.21	12.21
S-SBA-15/PMMA	100.8	0.38	12.41
M-S-SBA-15	236.8	0.92	13.80
M-S-SBA-15/PMMA	179.0	0.74	12.97
MCM-41	1286.4	0.74	2.54
MCM-41/PMMA	398.2	0.36	3.92
M-MCM-41	16.6	0.05	7.10
M-MCM-41/PMMA	10.7	0.04	7.90
MCM-48	1336.3	0.78	2.49
MCM-48/PMMA	836.5	0.52	3.00
M-MCM-48	13.8	0.04	7.72
M-MCM-48/PMMA	11.3	0.04	7.52

TGA analysis

TGA and DTG curves for different MS, MS/PMMA and M-MS/PMMA composites are showed in Fig. 3. With the rise of temperature, the MS, M-MS, MS/PMMA and M-MS/PMMA composites have a small weight loss around 100°C, which is attribute to the evaporation of water adsorbed in the MS. The MS has no obvious weight loss after 100°C, while the modified MS, M-R-SBA-15, M-S-S-SBA-15, M-MCM-41 and M-MCM-48 have a noteworthy weight loss between 100—800°C, these are 15.54%, 13.11%, 15.11% and 12.70%, respectively, which demonstrates that KH550 silane coupling agent has been well grafted onto different MS.

According to Fig. 3(c, d), by calculating the residual amount at 800°C, the weight loss of the R-SBA-15/PMMA, S-SBA-15/PMMA, MCM-41/PMMA and MCM-48/PMMA composites are 17.34%, 32.28%, 22.38% and 33.49% respectively. The apparent enormous weight loss of MCM-48/PMMA shows that MCM-48 adsorbed more MMA monomer. In addition, the termination decomposition temperature of the R-SBA-15/PMMA is the largest and the thermal stability is the best.

As we can see in Fig. 3(e, f), according to the same method, the weight loss of M-R-SBA-15/PMMA, M-S-SBA-15/PMMA, M-MCM-41/PMMA, and M-MCM-48/PMMA composites are 21.6%, 22.81%, 25.48%, and 24.10%, respectively, it can be deduced that the PMMA amounts polymerizated in the pores of M-R-SBA-15, M-S-SBA-15, M-MCM-41 and M-MCM-48 are 6.06%, 9.70%, 10.37% and 11.10%, individually. When comparing the amount of PMMA inside the pore channel, due to KH550 modification, the M-MS resulted in small pore channels, leading to the small amount of PMMA inside the pore channels.

Fig. 4 shows the TG and DTG curves of PMMAs obtained by polymerization inside the channels of the MS and M-MS after etched with HF, and C-PMMA obtained by conventional RAFT polymerization. Typically, there are three stages of thermal weight loss peaks for C-PMMA obtained by conventional RAFT polymerization, the first stage of weight loss, between 145°C—210°C, due to double bond breakage resulting from the termination of radical disproportionation; the second stage of weight loss, between 260°C—350°C, the decomposition of the short chain of PMMA generated by coupling termination; and the third stage of weight loss, between 320°C—420°C, the PMMA main chain random chain breakage decomposition. Compared to the C-PMMA, the initial thermal decomposition temperature of PMMA obtained from internal pore polymerization is obviously higher, especially the initial and termination thermal decomposition temperatures of the products from polymerization in M-MS are increased by about 80—100°C. The thermal decomposition of the polymer backbone is mainly present, while the less weight loss of the short chains of PMMA generated by disproportionation termination occurs due to the fact that the diffusion of free radicals is inhibited by the restricted effect of the pore channel, thus suppressing the chain termination reaction of RAFT solution polymerization.

FT-IR analysis

The structures of the obtained MS and M-MS and their composites were confirmed by FT-IR spectroscopy (Fig. 5 and Fig. 6). From Fig. 5(a), comparing pure MS, the M-MS show new characteristic peaks at 3356 and 1577 cm^{-1} corresponding to —NH_2 and —NH— respectively, which proves that KH550 successfully modified the MS [37]. From Fig. 5(b, c), the MS/PMMA and M-MS/PMMA composites not only retain the characteristic absorption peaks at 3430, 1080, 796 and 461 cm^{-1} of the MS corresponding to stretching and bending vibrations of Si—OH, Si—O—Si, and Si—O bonds, respectively, illuminating the presence of the SBA-15 framework [38,39], but new characteristic absorption peaks also appear at 2953 and 1731 cm^{-1}, which are the characteristic absorption peaks of carbonyl —C=O and the stretching vibration absorption peaks of methyl—CH_3 of PMMA in the composites, indicating that the MMA has adsorbed into the pore and undergone polymerization. [40]

After etching the MS/PMMA and M-MS/PMMA composites, the resulting product PMMA shows the same characteristic peaks as the PMMA obtained by conventional RAFT polymerization of MMA. In addition, the FT-IR spectra of polymer obtained from within and external of the pores show no absorbance at 1089 cm^{-1}, which is the characteristic peak to the Si–O–Si group, indicating a complete removal of MS [20,41].

GPC analysis

Molecular weight and molecular weight distribution of PMMAs obtained by RAFT polymerization inside the pores of the MS and M-MS, and by conventional RAFT polymerization are showed in Tab. 2. It is observed that the PMMAs obtained by RAFT polymerization inside the channel of the MS and M-MS exhibit a several times higher molecular weight than PMMA by the conventional RAFT polymerization, due to the much lower chance of termination of free radicals within the restricted pore channels [42]. The largest increase in number-average molecular weight (13.9—fold) is obtained within the pore channels of spherical SBA-15. The molecular weights of the PMMAs obtained from the R-SBA-15 and S-SBA-15 pores were larger than those of the modified M-SBA-15, but smaller molecular weight distribution, owing to the effect of the silane coupling agent on the surface of the modified SBA-15 [43].

The PMMAs obtained inside the unmodified MCM-41 and MCM-48 pores possess lower molecular weight and larger molecular weight distribution than these from modified MCM-41 and MCM-48, although the molecular weight distribution was still in the narrow category. [44]

Tab. 2 Molecular weight and molecular weight distributions of PMMAs obtained in the channels of MS and M-MA, and conventional PMMA by RAFT polymerization

Samples	number-average molecular weight $(M_n \times 10^4)$	weight-average molecular weight $(M_w \times 10^4)$	molecular weight distribution index (PDI)
PMMA in R-SBA-15	6.75	8.91	1.32
PMMA in M-R-SBA-15	1.69	2.79	1.65
PMMA in S-SBA-15	8.78	12.72	1.45
PMMA in M-S-SBA-15	3.33	5.75	1.73
PMMA in MCM-41	2.79	3.62	1.30
PMMA in M-MCM-41	4.53	5.45	1.20
PMMA in MCM-48	4.60	5.72	1.24
PMMA in M-MCM-48	7.43	8.37	1.13
C-PMMA	0.63	0.82	1.29

^{1}H NMR analysis

Typical ^{1}H NMR spectra of PMMAs obtained from conventional RAFT polymerization and PMMA in R-SBA-15 are depicted in Fig. 7. The peaks at 0.81–1.27, 1.60–1.90 and 3.60 ppm are assigned to the protons in the methyl, methylene and methoxy group of PMMA, respectively. In addition, triplet peaks at 0.84–1.25 ppm are assigned to proton of syndiotactic, atactic and isotactic in α-CH_3 with the direction of the shift value increase and stereoregularity data of all PMMA are summarized in Tab. 3 [45]. A relevant nanochannel effect on the polymer stereoregularity is observed in our polymerization system. PMMA in MCM-48 has the most significant reduction in the proportion of syndiotactic structures, yielding the highest isotactic PMMA. Whereas the sequence distribution of PMMA in R-SBA-15 does not change much owing to their large pore sizes and different wall thicknesses[19]. This further confirms the confinement effect of MS on monomer polymerization.

Tab. 3 Configurational sequence distribution of PMMA in SBA-15 by RAFT

Samples	rr(%)	mr(%)	mm(%)
C-PMMA	52.08	33.33	14.58
PMMA in R-SBA-15	50.76	33.50	15.74
PMMA in M-R-SBA-15	43.86	25.00	31.14
PMMA in S-SBA-15	48.08	31.73	20.19
PMMA in M-S-SBA-15	40.81	24.90	34.29
PMMA in MCM-41	44.05	29.96	28.87
PMMA in M-MCM-41	55.56	27.78	16.67
PMMA in MCM-48	33.00	19.80	47.19
PMMA in M-MCM-48	42.02	28.15	29.83

Conclusion

RAFT polymerization of MMA inside the pore channels of MS or M-MS was successfully conducted. The resulting composites still retain their original morphological structure, but the specific surface areas and pore volumes of the M-MS and composites are reduced. Compared with C-PMMA obtained by conventional RAFT solution polymerization, the molecular weights of the PMMA inside the pore channel are several times or even a dozen times higher than that of conventional C-PMMA, as an example, the number average molecular weight of the PMMA obtained inside the S-SBA-15 pore channel increase by 13.9 times. However, the molecular weight distributions keep at s narrow range, and the isotactic ratio of the polymer increases significantly. The initial thermal decomposition temperature was significantly increased, especially the decomposition temperature of PMMA obtained in the modified MS was increased by 80–100°C. This work provided a novel approach to design of polymer microstructure for a wider application.

Declarations

Conflicts of interest

There are no conflicts to declare.

Acknowledgements

The authors greatly acknowledge the financial support from the Natural Science Foundation of China (No.21664005).

Author Contributions

Conceptualization, F. Zhang; Data curation, Y. Wei; Formal analysis, Y. Wei, T. Xue, F. Zhang and C. Yu; Validation, T. Xue; Writing-original draft, T. Xue; Writing-review and editing, F. Zhang and C. Yu. All authors have read and agreed to the published version of the manuscript

References

1. S. Matsuura, R. Ishii, T. Itoh, S. Hamakawa, T. Tsunoda, T. Hanaoka,F. Mizukami, On-chip encapsulation of lipase using mesoporous silica: A new route to enzyme microreactors. Mater. Lett. **63**(28), 2445-2448 (2009)
2. M. de Fátima V. Marques, O.F.C. da Silva, A.C.S.L.S. Coutinho,A.S. de Araujo, Ethylene polymerization catalyzed by metallocene supported on mesoporous materials. Polym. Bull. **61**(4), 415-423 (2008)
3. F. Márquez, R. Roque-Malherbe, J. Ducongé,W. del Valle, Polymerization of aniline in the channels of micro- and mesoporous materials. Surf. Interface Anal. **36**(8), 1060-1063 (2004)
4. S. Jimenez-Falcao, D. Torres, P. Martinez-Ruiz, D. Vilela, R. Martinez-Manez,R. Villalonga, Sucrose-Responsive Intercommunicated Janus Nanoparticles Network. Nanomater. **11**(10), 2492-2502 (2021)
5. E. Pellicer, J. Sort, Frontiers in Mesoporous Nanomaterials. Nanomater. **6**(1), 15-18 (2016)
6. Y. Jeong, S.S. Park, A.R. Sung,C.S. Ha, Comparative Studies on Drug Delivery Behavior of Mesoporous Silicas. Mol. Cryst. Liq. Cryst. **600**(1), 70-80 (2014)
7. P. Singh, P.K. Maiti, K. Sen, Pristine and modified-mesoporous alumina: molecular assistance-based drug loading and sustained release activity. Bull. Mater. Sci. **43**(1), 56-64 (2020)
8. A. Kierys, R. Zaleski, M. Grochowicz, M. Gorgol,A. Sienkiewicz, Polymer–mesoporous silica composites for drug release systems. Microporous Mesoporous Mater. **294**, 109881 (2020)
9. J. Choi, V. Valtchev, T. Moteki,M. Ogura, Phase Change Material-Containing Mesoporous Zeolite Composite for Adsorption Heat Recovery. Adv. Mater. Interfaces. **8**(4), 2001085 (2021)
10. J. Du, L. Liu, Y.F. Yu, Y. Zhang,A.B. Chen, Mesoporous carbon materials with different morphology for pesticide adsorption. Appl. Nanosci. **10**(1), 151-157 (2020)

11. Y.M. Hu, J. Florek, D. Larivière, F.-G. Fontaine,F. Kleitz, Recent Advances in the Separation of Rare Earth Elements Using Mesoporous Hybrid Materials. Chem Rec. **18**(7-8), 1261-1276 (2018)
12. X.X. Li, K.H. Row, Separation of Polysaccharides by SEC Utilizing Deep Eutectic Solvent Modified Mesoporous Siliceous Materials. Chromatographia. **80**(8), 1161-1169 (2017)
13. J. Jung, O. Keller, Photon wave-mechanical theory of single-photon diffraction from a mesoscopic hole. J PHYS B-AT MOL OPT. **54**(4), 045401 (2021)
14. B. Rivas-Mundiña, Z. Vargas-Osorio, S. Yáñez-Vilar, M. Rizk, Y. Piñeiro, M. Pérez-Sayáns,J. Rivas, Hybrid mesoporous nanostructured scaffolds as dielectric biosimilar restorative materials. Bio-Med. Mater. Eng. **32**, 243-255 (2021)
15. N. Corrigan, K. Jung, G. Moad, C.J. Hawker, K. Matyjaszewski,C. Boyer, Reversible-deactivation radical polymerization (Controlled/living radical polymerization): From discovery to materials design and applications. Prog. Polym. Sci. **111**, 101311 (2020)
16. M. Kamigaito, M. Sawamoto, Synergistic Advances in Living Cationic and Radical Polymerizations. Macromolecules. **53**(16), 6749-6753 (2020)
17. M.D. Nothling, Q. Fu, A. Reyhani, S. Allison-Logan, K. Jung, J. Zhu, M. Kamigaito, C. Boyer,G.G. Qiao, Progress and Perspectives Beyond Traditional RAFT Polymerization. Adv. Sci. **7**(20), 2001656 (2020)
18. N.P. Truong, G.R. Jones, K.G.E. Bradford, D. Konkolewicz,A. Anastasaki, A comparison of RAFT and ATRP methods for controlled radical polymerization. Nat. Rev. Chem. **5**(12), 859-869 (2021)
19. X. Xu, Y.N. Zeng, C.L. Yu,F.A. Zhang, Controlled RAFT polymerization of MMA in confined space of various pore sizes of SBA-15. J. Porous Mater. **27**(1), 95-105 (2020)
20. M.S. Chen, L.M. Qin, Y.L. Liu,F.A. Zhang, Controllable preparation of polymer brushes from mesoporous silica SBA-15 via surface-initiated ARGET ATRP. Microporous Mesoporous Mater. **263**, 158-164 (2018)
21. T. Joshi, L. Nebhani, Light-regulated growth of polymer chains from the surface of RAFT agent primed mesoporous silica nanoparticles. Surf. Interfaces. **29**, 101764 (2022)
22. H. Dan, Y. Ding, X.R. Lu, F.T. Chi,S.B. Yuan, Adsorption of uranium from aqueous solution by mesoporous SBA-15 with various morphologies. J. Radioanal. Nucl. Chem. **310**(3), 1107-1114 (2016)
23. Y.N. Zeng, S.X. Liu, Y.Q. Xu,F.A. Zhang, Investigation of RAFT polymerization in mesoporous SBA-15 by using various monomers. J. Porous Mater. **27**(3), 659-669 (2020)
24. M. Moritz, M. Geszke-Moritz, Sulfonic Acid Derivative-Modified SBA-15, PHTS and MCM-41 Mesoporous Silicas as Carriers for a New Antiplatelet Drug: Ticagrelor Adsorption and Release Studies. Materials. **13**(13), 2913-2936 (2020)
25. D.W. Gao, A.J. Duan, X. Zhang, Z. Zhao, H. E, J.M. Li,H. Wang, Synthesis of NiMo catalysts supported on mesoporous Al-SBA-15 with different morphologies and their catalytic performance of DBT HDS. Appl. Catal., B. **165**, 269-284 (2015)
26. D.Y. Zhao, J.Y. Sun, Q.Z. Li,G.D. Stucky, Morphological Control of Highly Ordered Mesoporous Silica SBA-15. Chem. Mater. **12**(2), 275-279 (2000)

27. D.Y. Zhao, J.L. Feng, Q.S. Huo, N. Melosh, H. Fredrickson Glenn, F. Chmelka Bradley,D. Stucky Galen, Triblock Copolymer Syntheses of Mesoporous Silica with Periodic 50 to 300 Angstrom Pores. Science. **279**(5350), 548-552 (1998)
28. K. Schumacher, M. Grün, K.K. Unger, Novel synthesis of spherical MCM-48. Microporous Mesoporous Mater. **27**(2), 201-206 (1999)
29. Z.B. Wei, R. Bai, F.A. Zhang, Mma Solution Polymerization in the Channels of Modifiled Mesoporous Molecular Sleves SBA-15. Acta Polym. Sin., 119-121 (2013)
30. Y.G. Wang, F.Y. Zhang, Y.Q. Wang, J.W. Ren, C.L. Li, X.H. Liu, Y. Guo, Y.L. Guo,G.Z. Lu, Synthesis of length controllable mesoporous SBA-15 rods. Mater. Chem. Phys. **115**(2), 649-655 (2009)
31. Y. Miyake, T. Kato, The Formation Process of Spherical Mesoporous Silica with Reverse Nanostructure of MCM41 in a Two-phase System. J. Chem. Eng. Jpn. **38**(1), 60-66 (2005)
32. Y. Liu, J. Qiu, Y.H. Jiang, Z.C. Liu, M.J. Meng, L. Ni, C.C. Qin,J.B. Peng, Selective Ce(III) ion-imprinted polymer grafted on Fe3O4 nanoparticles supported by SBA-15 mesopores microreactor via surface-initiated RAFT polymerization. Microporous Mesoporous Mater. **234**, 176-185 (2016)
33. C. Serre, A. Auroux, A. Gervasini, M. Hervieu,G. Férey, Hexagonal and Cubic Thermally Stable Mesoporous Tin(IV) Phosphates with Acidic and Catalytic Properties. Angew. Chem., Int. Ed. **41**(9), 1594-1597 (2002)
34. D. Pérez-Quintanilla, S. Gómez-Ruiz, Ž. Žižak, I. Sierra, S. Prashar, I. del Hierro, M. Fajardo, Z.D. Juranić,G.N. Kaluđerović, A New Generation of Anticancer Drugs: Mesoporous Materials Modified with Titanocene Complexes. Chem. Eur. J. **15**(22), 5588-5597 (2009)
35. A. Benhamou, M. Baudu, Z. Derriche,J.P. Basly, Aqueous heavy metals removal on amine-functionalized Si-MCM-41 and Si-MCM-48. J. Hazard. Mater. **171**(1), 1001-1008 (2009)
36. M. Anbia, N. Mohammadi, K. Mohammadi, Fast and efficient mesoporous adsorbents for the separation of toxic compounds from aqueous media. J. Hazard. Mater. **176**(1), 965-972 (2010)
37. M. Kruk, M. Jaroniec, C.H. Ko,R. Ryoo, Characterization of the Porous Structure of SBA-15. Chem. Mater. **12**(7), 1961-1968 (2000)
38. F.A. Zhang, M. Luo, Z.J. Chen, Z.B. Wei,T.J. Pinnavaia, Effects of mesoporous silica particles on the emulsion polymerization of methyl methacrylate. Polym. Eng. Sci. **54**(12), 2746-2752 (2014)
39. M. Choi, F. Kleitz, D. Liu, H.Y. Lee, W.-S. Ahn,R. Ryoo, Controlled Polymerization in Mesoporous Silica toward the Design of Organic−Inorganic Composite Nanoporous Materials. J. Am. Chem. Soc. **127**(6), 1924-1932 (2005)
40. M.S. Chen, H.W. Zhou, L. Zhou,F.A. Zhang, Confined polymerization: ARGET ATRP of MMA in the nanopores of modified SBA-15. Polymer. **114**, 180-188 (2017)
41. C. Wang, W.L. Gu, J.H. Li, D.Y. Huang, W.P. Lu, P. Huang,M. Wu, Synergic Deoxy Reforming of Cellulose and Fatty Oil Using Molecular-Sieve-Supported Molybdenum Carbide and Tungsten Carbide towards Hydrocarbon-Rich Oil for Fuels. Energy Technol. **5**(12), 2216-2225 (2017)

42. S.M. Ng, S.i. Ogino, T. Aida, K.A. Koyano,T. Tatsumi, Free radical polymerization within mesoporous zeolite channels. Macromol. Rapid Commun. **18**(12), 991-996 (1997)
43. H.-C. Lee, J. Hwang, U. Schilde, M. Antonietti, K. Matyjaszewski,B.V.K.J. Schmidt, Toward Ultimate Control of Radical Polymerization: Functionalized Metal–Organic Frameworks as a Robust Environment for Metal-Catalyzed Polymerizations. Chem. Mater. **30**(9), 2983-2994 (2018)
44. O. Olkhovyk, M. Jaroniec, Adsorption Characterization of Ordered Mesoporous Silicas with Mercury-Specific Immobilized Ligands. Adsorption. **11**(1), 685-690 (2005)
45. N. Adiram-Filiba, A. Schremer, E. Ohaion, M. Nadav-Tsubery, T. Lublin-Tennenbaum, K. Keinan-Adamsky,G. Goobes, Ubiquitin immobilized on mesoporous MCM41 silica surfaces – Analysis by solid-state NMR with biophysical and surface characterization. Biointerphases. **12**(2), 02D414 (2017)

Figures

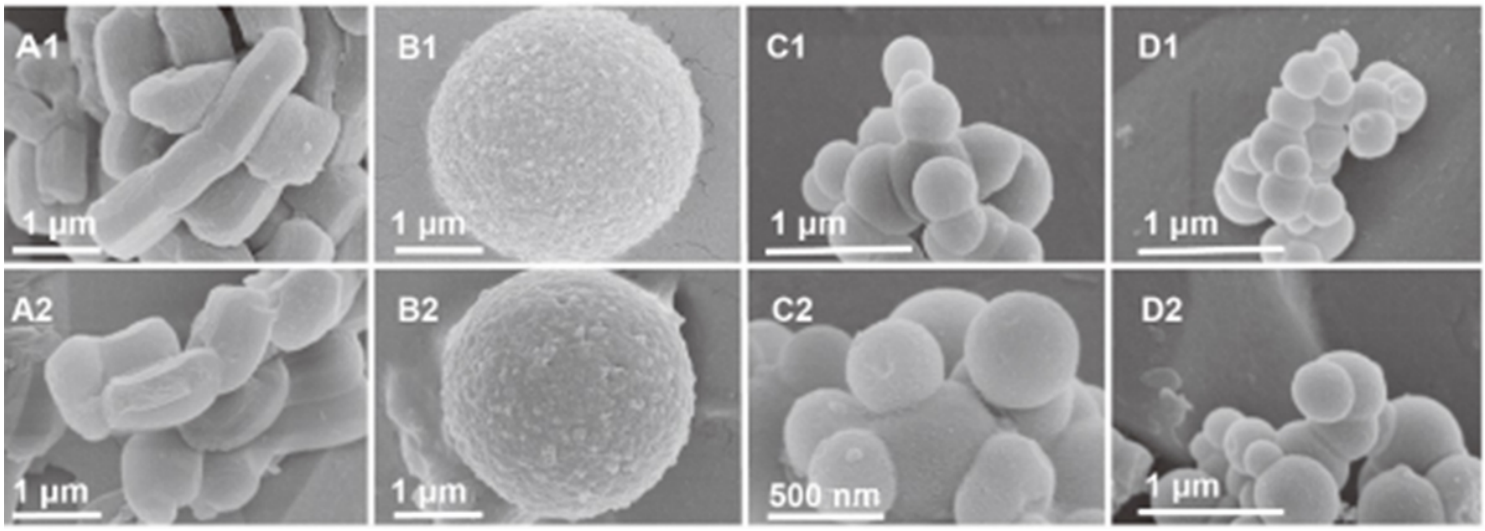

Figure 1

SEM images of different mesoporous silica, MS-PMMA nanocomposites

(A1: R-SBA-15, B1: S-SBA-15, C1: MCM-41, D1: MCM-48;

A2: R-SBA-15/PMMA, B2: S-SBA-15/PMMA, C2: MCM-41/PMMA, D2: MCM-48/PMMA)

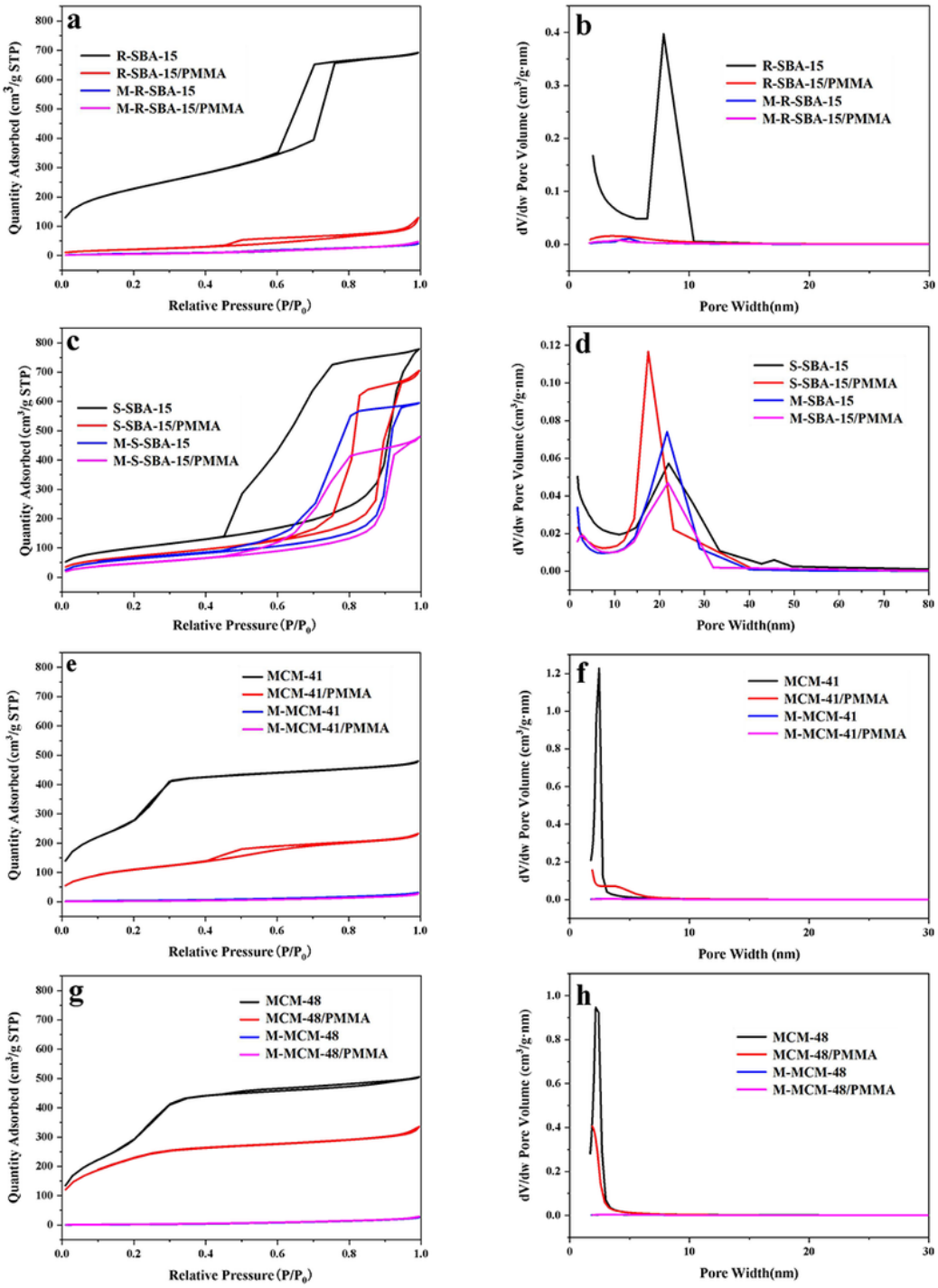

Figure 2

Nitrogen adsorption/desorption isotherms and pore size distribution of MS, MS/PMMA composites and M-MS/PMMA composite

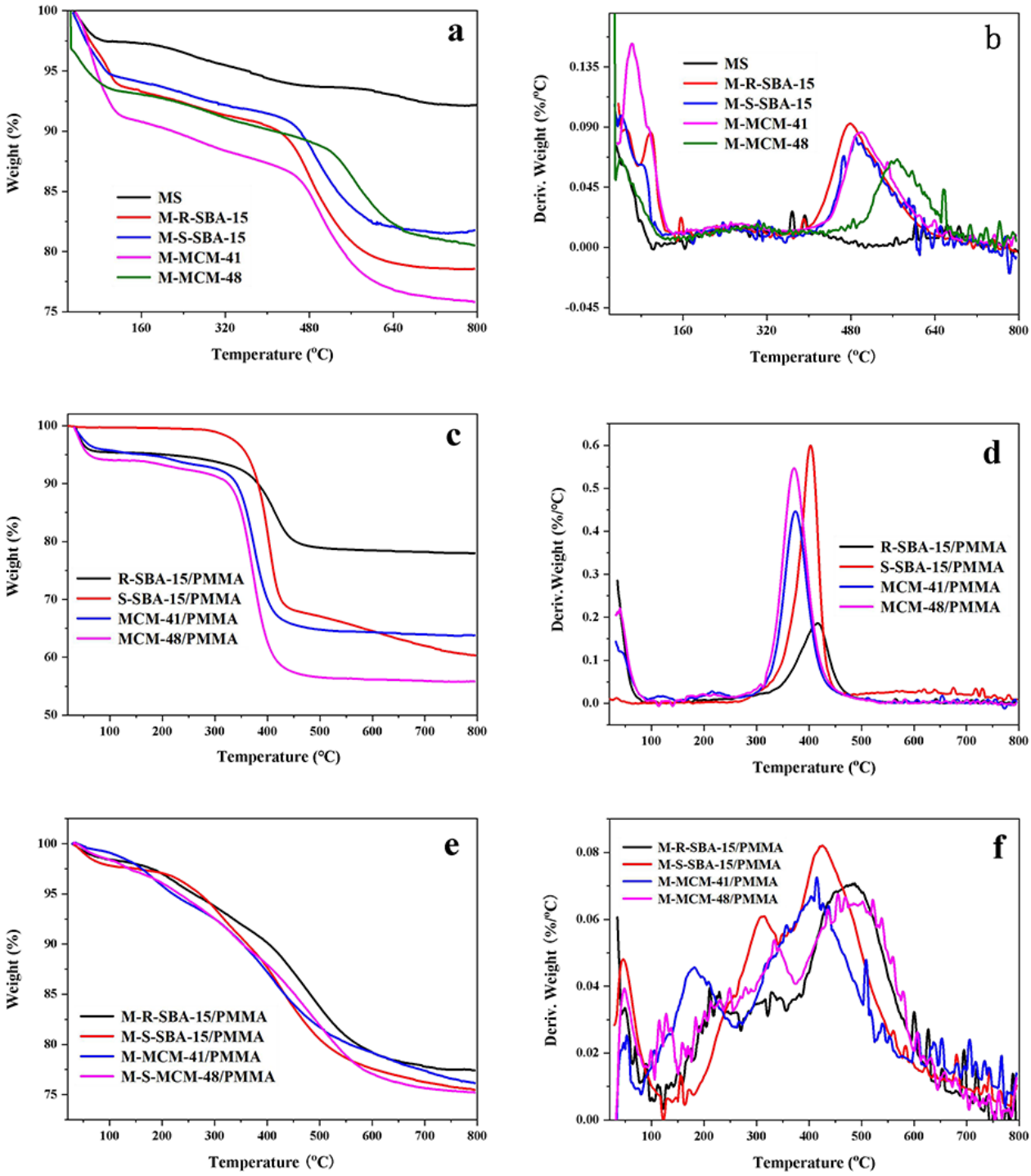

Figure 3

TG and DTG curves of MS and M-MS (a, b), MS/PMMA (c, d) and M-MS/PMMA composites (e, f)

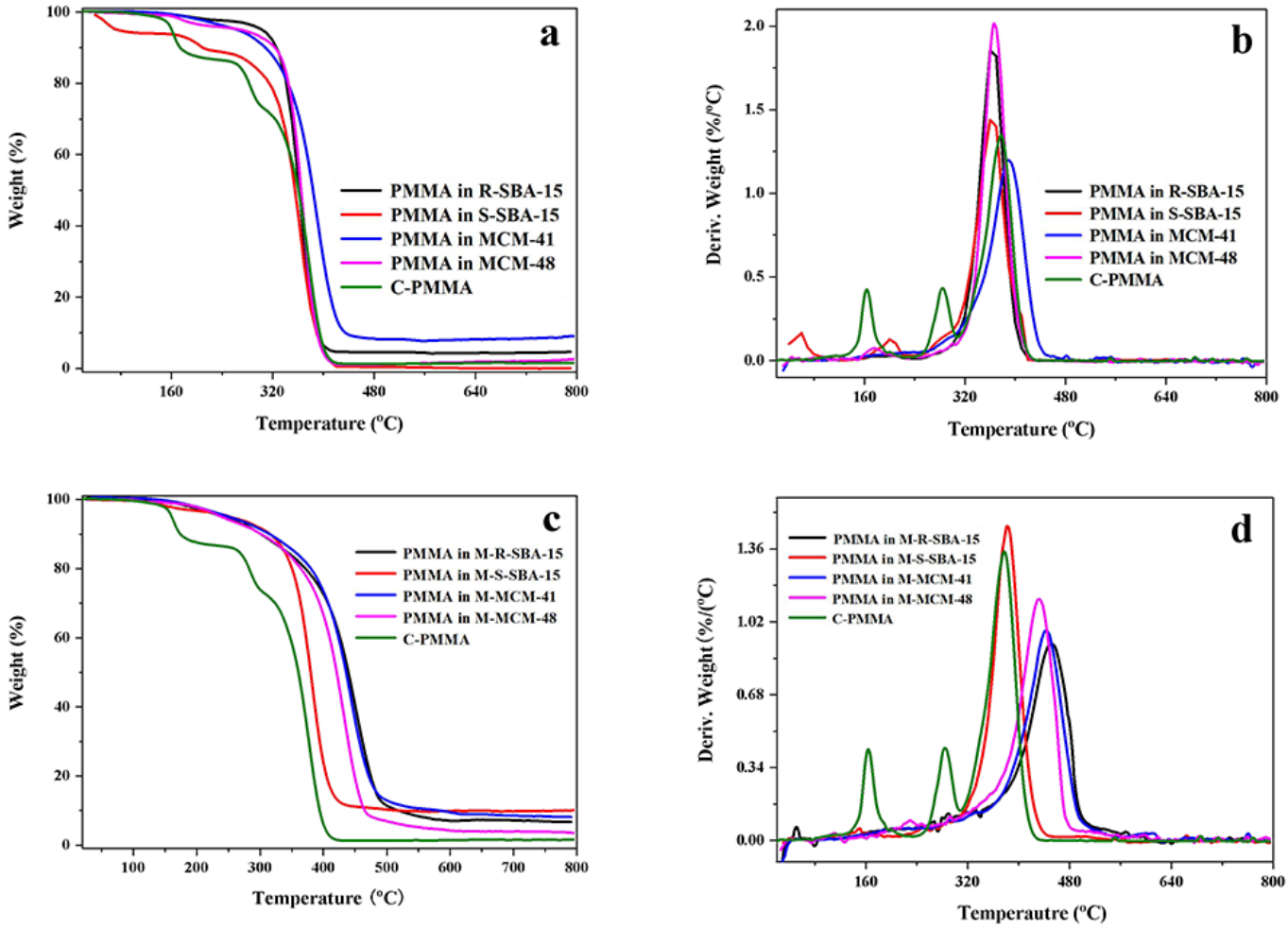

Figure 4

TG and DTG curves of PMMA in MS and C-PMMA by RAFT

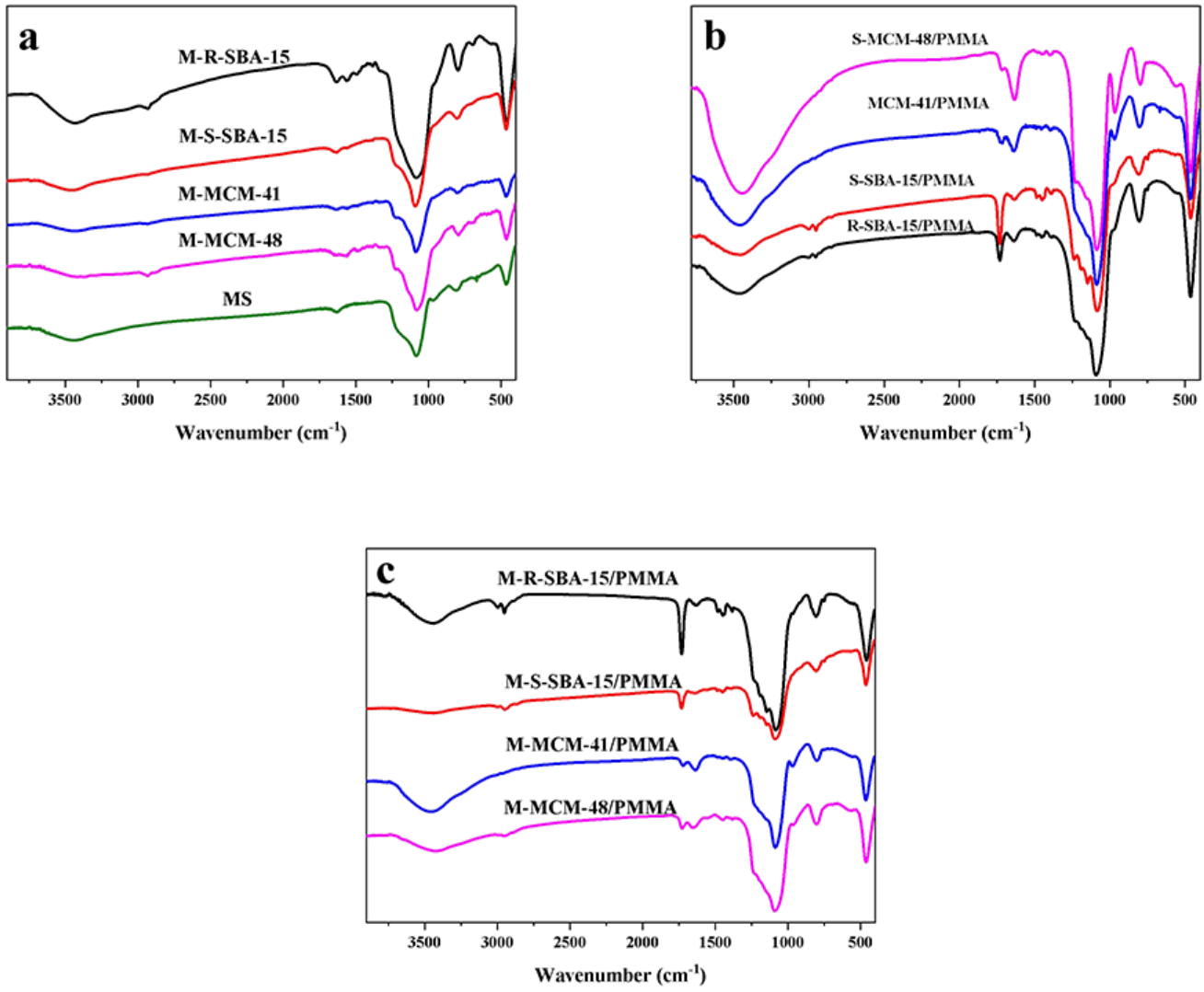

Figure 5

FT-IR spectra of MS, M-MS, MS/PMMA and M-MS/PMMA composites

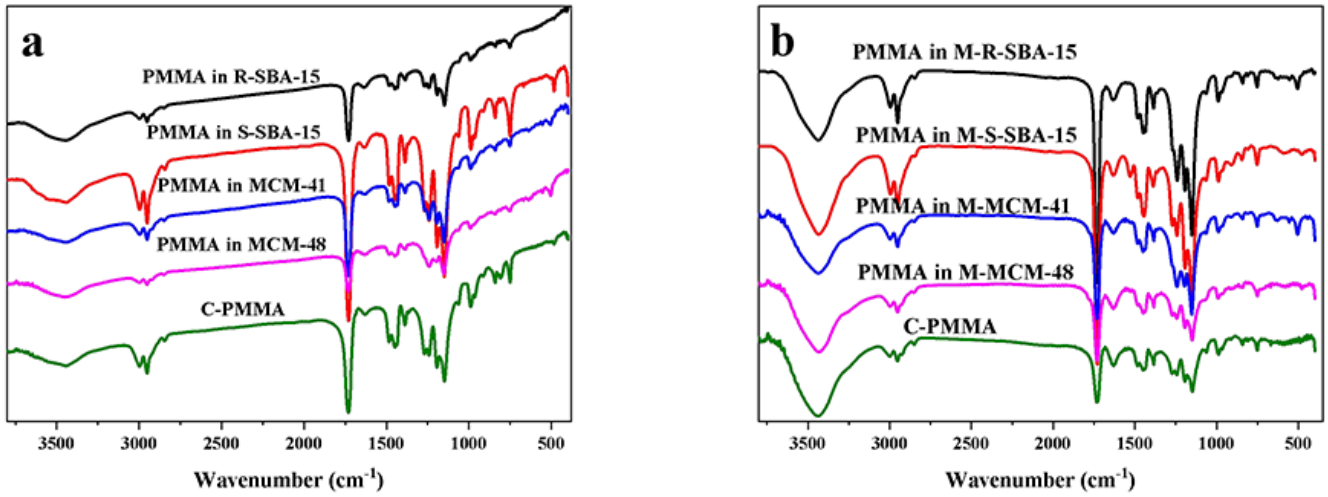

Figure 6

FT-IR spectra of PMMA obtained in the channels of SBA-15 and conventional PMMA by RAFT polymerization

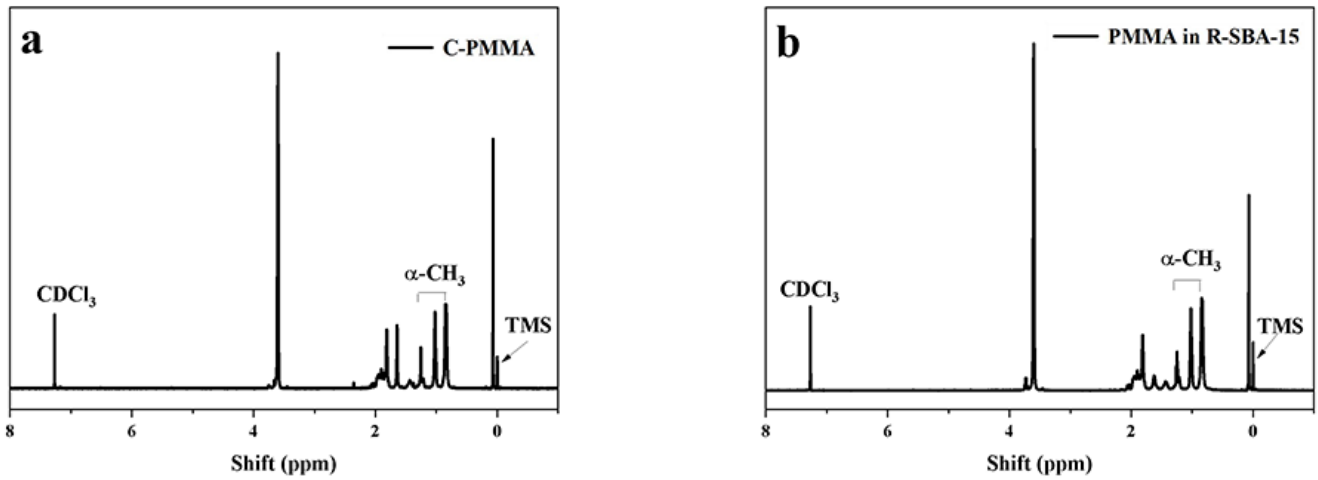

Figure 7

^{1}H-NMR of PMMA and PMMA in R-SBA-15